COBEM 2021 26th International Congress of Mechanical Engineering
November 22-26, 2021, Virtual Congress, Brazil

# COB-2021-1727
# MATERIAL CHARACTERIZATION AND ANALYSIS OF CRITICAL FAILURE IN EGR COMPONENT FOR DIESEL PICKUP TRUCKS

**Elberton Santos Castro**
University Center-UNA, 59, Alameda Paulina Margonari st., Uberlândia/MG
elbertonscastro@hotmail.com

**Felipe dos Anjos Rodrigues Campos**
Federal University of Uberlândia-UFU, Laboratory for Machining Research and Learning-LEPU, 2121, João Naves de Ávila av., Uberlândia/MG
filipin_anjos@hotmail.com

**Maksym Ziberov**
University of Brasília, Technology College, 70910-900, Via L3 Norte av., Brasília/DF
mziberov@unb.br

**André Rezende de de Figueiredo Oliveira**
Federal University of Uberlândia-UFU, Laboratory for Machining Research and Learning-LEPU, 2121, João Naves de Ávila av., Uberlândia/MG
arfoliveira@ufu.br

***Abstract.*** *Current environmental concerns press the automotive industry to produce more efficient engines, as exemplified by the exhaust gas recirculation system (EGR) in Diesel vehicles. Part of the exhaust gases is reintroduced in the combustion chamber mixed with the intake air. However, the hot gasses must be previously cooled down indirectly in a radiator, through which circulates water from the engine cooling system. The combination of high temperatures in the radiator tubes and possible presence of residual stress from the assembly processes might promote crack formation, which may causes serious leakages. This work was based on the failure analysis of a recurrent leakage problem in the EGR radiator of Diesel pickup trucks. A case study was conducted with damaged parts, which were examined by dye penetrant inspection and leakage test with water at 1 bar and 100 °C. Small cracks were observed in the joints of the tubes with the radiator baffles, likely due to crevice corrosion. Pit corrosion was also verified along the tubes, in the form of small holes visible only by optic microscopy. Scanning electron microscopy (SEM), energy dispersive x-ray spectroscopy (EDS) and hardness tests were used to characterize the stainless steel alloys of the EGR radiator. The corroded surface presented high content of adhered aluminum oxide, usually formed by the reaction contaminated water and metal parts. The chemical composition and hardness of the tubes also indicates the application of stainless steel of series 300, but without the minimum amount of nickel recommended by the ASTM standards. Based in the results, it was suggested for the manufacturer to change the type or acquisition source of the stainless steel in the tubing, in order to reduce maintenance events and improve brand reliability.*

***Keywords:*** *failure analysis, exhaust gas recirculation, dye penetrant test, stainless steel, corrosion*

## 1. INTRODUCTION

The greatest environmental concerns in recent years have motivated government agencies to create increasingly restrictive legislation and control mechanisms in relation to pollution caused by combustion vehicles. As a recent example, there are the resolutions 490 and 492 of the Brazilian Council for the Environment (CONAMA, 2018a; CONAMA, 2018b), linked to the Ministry of the Environment, which reduce the maximum pollution limits for new light and heavy vehicles to be sold in the coming years.

In this sense, the automotive industry has been pressured to develop more efficient engines and incorporate new systems to control and reduce emissions. In diesel vehicles this can be exemplified by the Diesel particulate filter (DPF), the selective catalytic reduction device (SCR) and the gas recirculation system (EGR), all of which work with the exhaust gases. The first aims at trapping small solid particles that are not completely burned through a ceramic filter. In high rotation conditions, the higher temperature of the gases disintegrates the particles accumulated in the filter, regenerating it. The second promotes the reduction of NOx-type oxide emissions from catalytic reactions with urea compounds (Yuan et. al., 2015), which promote the transformation into gaseous nitrogen of nitrogenous oxides that are harmful to the ozone layer and cause acid rain.

The EGR device also works to reduce the emissions of these oxides and is already a common item in Diesel vehicles sold in Brazil. It reuses part of the exhaust gases by mixing them with the intake air. Thus, by making the mixture less rich in oxygen, lower temperatures in the combustion chamber are obtained, reducing the formation of NOx (Zamboni and Capobianco, 2012). Normally, before mixing, the recirculated gases are cooled in a radiator through which water from the engine's cooling system passes. The main components and their position in the engine can be seen in Fig. 1.

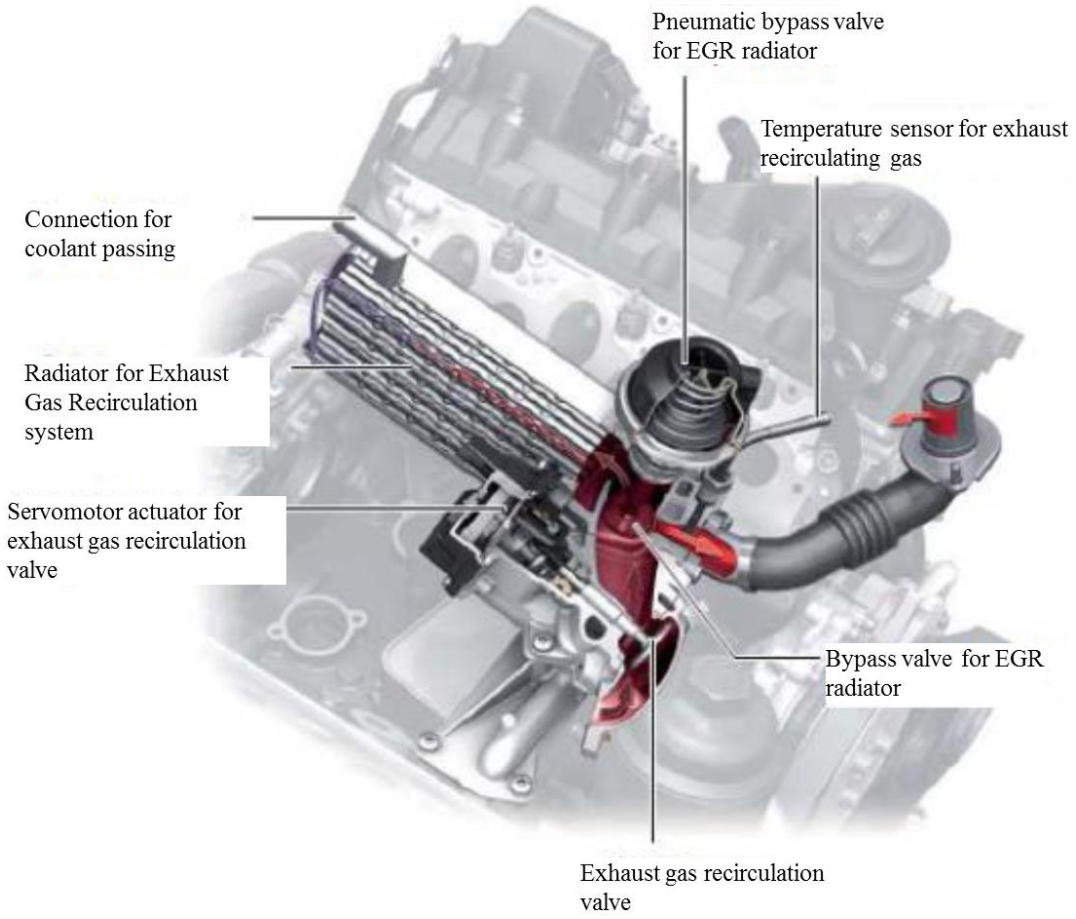


Figure 1. Main components of the EGR system and their position in the engine.

In such parts that work under high thermal gradients and in contact with highly reactive combustion gases, corrosion becomes an important type of wear. As explained by Janikowski and Blessman (2008), even stainless steels from the 300 series are susceptible to cracking due to stress corrosion in the presence of chloride. This may result from the combination of three factors: trace amounts of chlorides, high stresses, and temperatures above 65 °C. A variety of stress sources are possible: residual stresses from the tube manufacturing, thermally induced stresses, pressure induced stresses, and other mechanical stresses from operations. In the case of tubing for heat exchangers, all these stress sources are present and contribute to crack formation. Furthermore, the alloy's chemical composition has already been discussed as an important factor for verification, since many current stainless steel suppliers fail to meet the material standard requirements (Janikowski, 2012).

According to Papavinasam (2014), inspection of corrosion is already a complicated task, since most of the times the critical components cannot be easily inspected. However, in the case of part failure in automobile industry, manufacturers usually promote a thorough root cause analysis to verify liabilities in the design or manufacturing processes of the part, which could lead to expensive recalls if unattended. Especially in the case of premature corrosion wear, firstly, the supplied material must be checked against the standard requirements for chemical stability. Secondly, the structural integrity is typically assessed for cracks or defects through use of non-destructive tests such as die penetrant liquid, magnetic particles, eddy current and ultrasonic, or miscellaneous test, such as hydrostatic or tightness test, for which DIN EN 1779 (2019) provides a reference of the more adequate type. In general, as stated in ASTM A1047/A1047M-05 (2019), any visible passage of fluid through the wall of the specimen shall constitute failure.

Within these regards, this work was based on the failure analysis for a common problem observed in the EGR radiator of a national diesel truck manufacturer. In many cases the vehicles had a reduction in the coolant level, which could lead to engine overheating and consequent catastrophic failure. This problem was recurrently observed, having as one of the main causes leaks present in this recirculating gas radiator. A case study was carried out with condemned parts, applying

penetrating liquid and performing a leakage test with hot water. The main points of leaks were observed in the fixation regions of the internal tubes of the heat exchanger and in small holes originated from pits of corrosion. Surface hardness analysis and energy dispersive X-ray spectroscopy (EDS) in a scanning electron microscope (SEM) were performed to characterize the material of the radiator housing and inner tubes. The tests indicated characteristics compatible with those of stainless steels of the 300 series, however, outside the composition ranges recommended by ASTM standards for this type of application.

## 2. METHODOLOGY

In order to verify the origin of the leaks, a part was sectioned transversally and submitted to the tightness test following the general guidelines of ASTM A1047/A1047M-05 (2019). The pressurization was carried using water vapor condensate at a pressure of 1 bar and a temperature of 100 °C. The first value was measured through a pressure gauge located in the steam trap valve of the industrial steam circuit used. The second is the approximate temperature of boiling water, since the fluid released from the trap valve has just condensed. Piping from this circuit was welded to the inlet of the radiator box, while the outlet was welded to a valve, kept closed during testing. The diagram can be seen in Fig. 2 and represents the condition of the box in the vehicle, in which the water circulates inside the box, around the tubes, while the combustion gases pass through the inside of the tubes.


Figure 2. Diagram of the tightness test in the EGR radiator with water at 110 °C.

The EGR case was also examined by the liquid penetrant method, using a visible liquid, water washable, model VP30 from Metal Check. This was applied to the tubes and in the regions where they fit to the mirror of the EGR box, leaving it to act for 20 minutes and washing in sequence. The liquid penetrates the cracks by capillarity and washing removes the remaining excess. Metal Check's non-aqueous developer D70 was sprayed on surfaces, which the product was left on for 20 minutes to react with the penetrating liquid present in the cracks, visually enhancing them.

Electron microscopy images were taken of samples from the box and tubes on a Zeiss EVO MA10 microscope and chemical composition analysis by X-ray dispersion were obtained in an Oxford INCAx-act coupled detector. In addition, a sample of approximately 20 x 20 mm was cut from the EGR box, which was sanded with #600 sandpaper and polished with aluminum oxide of average grain size 1 µm, reaching the finishing shown in Fig. 3(a).

Hardness tests were performed on a Digimess 400.010 benchtop durometer using a 1/16" (1.58 mm) hardened steel ball as the penetrator. The Rockwell surface hardness test was performed with a load of 15 kg for 30 s, with an analog reading on the scale of the device. Samples from the EGR tubes were sawed as in Fig. 3b, and later cut and opened as in Fig. 3c to perform hardness tests. First, they were subjected to annealing by heating it in a muffle oven Quimis Q318M21 at 750 °C for 10 min and letting it cool inside the oven. However, due to the low thickness of the material, hardness still varied greatly and hindered the reliability of the results. The microstructure analysis of the tubes and sheet of the outer box of radiator were carried in different types of optical microscopes, including a Topcon B100-1 with objective lens 4x (PL L 4/0.10 160), for an amplification of 400 times, and a polarizing microscope BX53-P using objectives of 10x.

Chemical attack was used to differentiate the austenite grains, by using a solution of hydrochloric acid at 20 % concentration for 1 min and 3 min for the sheet and tubes, respectively. This is because the deformed tube material could not be sanded and polished as in the case of the first item, and the chemical attack was also used as means of cleaning it. Additionally, iron (III) chloride hexahydrate at 60 % weight was used in a second metallographic trial after grinding and polishing of a section of the tubes, for better observation of the grain boundaries at the tube sample, and a mix of 30 % nitric acid and 10 % hydrochloric was used in a third trial.

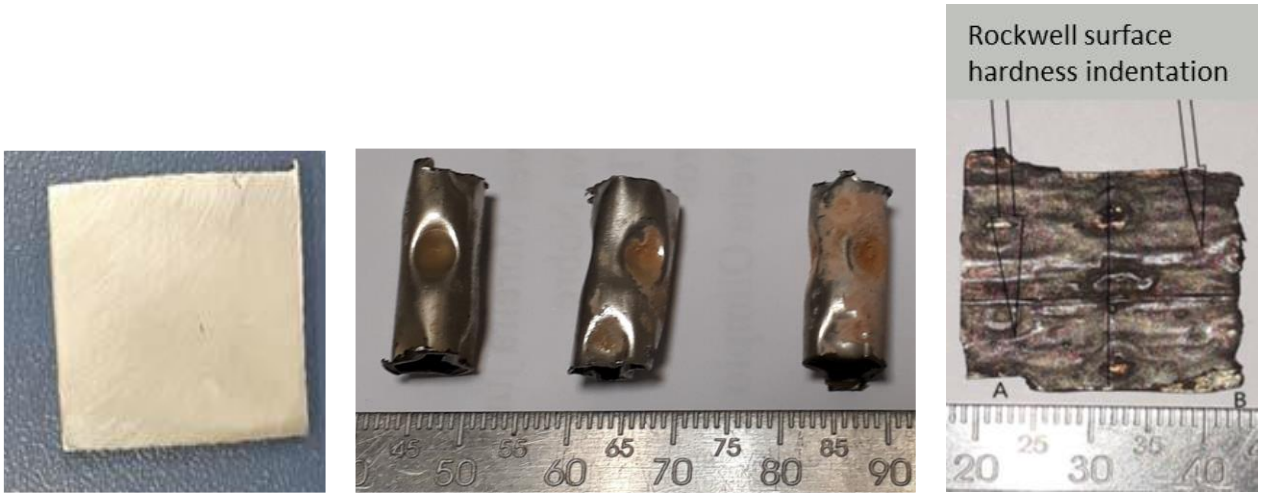


(a) (b) (c)

Figure 3. Samples for hardness testing of the EGR radiator box (a) and tubes (b), (c).

## 3. RESULTS AND DISCUSSION

During the tightness test with water at 110 °C, considerable leaks were noticed in the radiator end plates, around the fitting of the tubes. During the fabrication of the parts, to produce a tight closure, the tubes are expanded against the holes in the mirror, preferably by boring and welding. Thus, leaks can be related to the manufacturing processes used.

The use of penetrating liquid revealed the presence of cracks in the region where the mirror fits with the tubes, exemplified by the more intense red line shown in Fig. 4b, explaining the leaks observed. In both the boring and welding operations, residual stresses are common, which favors corrosion if the medium presents favorable characteristics (Mukahiwa et. al., 2019). In fact, in vehicle cooling systems, although manufacturers recommend the addition of appropriate coolant with additives that retard corrosion, many drivers do not change the fluid regularly or use tap water, which contains considerable amounts of chlorine and aluminum, between other ions. In this sense, the possible presence of these ions together with residual stresses and typical weld defects, such as inclusions and carbide precipitation in the grain boundaries, may have led to localized corrosion and caused these types of cracks observed.

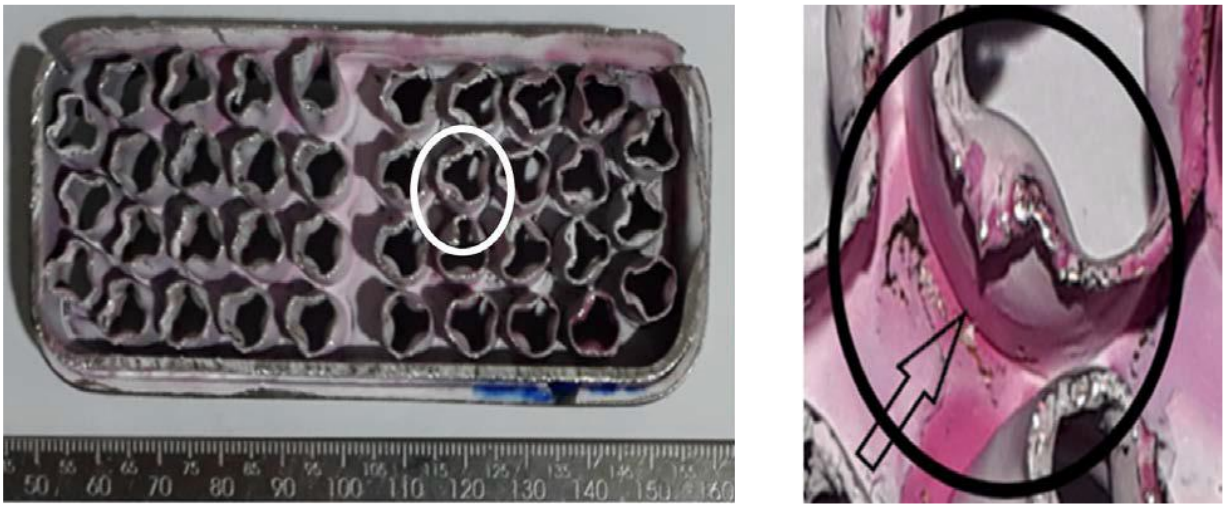

(a) (b)

Figure 4. (a) Mirror of the EGR radiator box (part of the box with the tubes were cut transversally). (B)

In addition, some pitting corrosion was found on the surface of the tubes, as shown in Fig. 5. This type of corrosion occurs locally and normally originates from the removal of the passivating layer, creating a galvanic cell where the point under corrosion acts as anode (Pradhan et. al., 2019). As this mechanism progresses mainly in terms of thickness, again the presence of chlorine and residual stresses, however low, can lead to the appearance of small holes in thin stainless steel plates (Zhu et. al., 2013). This process is further favored by the high temperature of the exhaust gases that circulate inside the tubes and is especially important when incrustations are present, as shown in Fig. 6. This way, the corroded material has low resistance and may be removed by coolant flow, taking off the passivating layer and exposing the bare metal to corrosion. This phenomenon is a strong indicator that the water was used by the vehicle owners were contaminated in some cases, since it contains a high content of aluminum and silicon oxides that usually make up the incrustations.

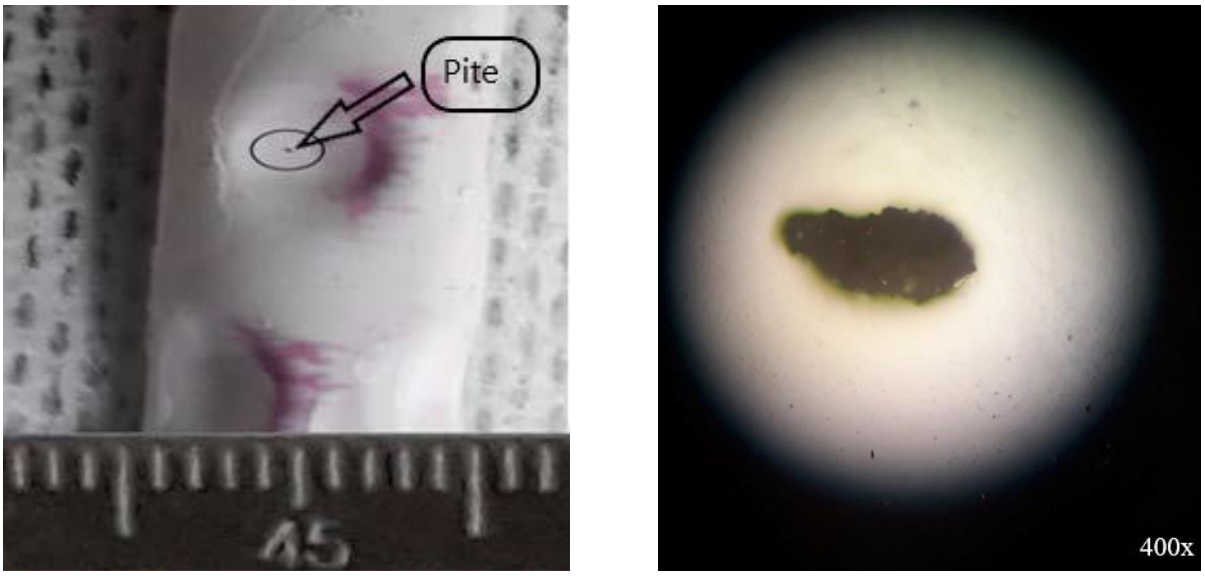


(a) (b)

Figure 5. (a) Corrosion pit revealed by penetrating liquid. (b) Microscope magnified image of the pit.


Figure 6. Incrustations formed inside the tubes of the EGR heat exchanger.

The analysis by electron microscopy of the tubes was carried out in two regions: oxidized, as shown in Fig. 7(a), and non-oxidized, shown in Fig. 7(b). Table 1 shows the respective chemical compositions of the points sampled by EDS. In the first region, high amounts of oxygen and aluminum can be seen, probably in the form of oxides adhering to the surface, which explains the visible aspect of encrusted material. These oxides form from salts dissolved in the water in the cooling system and are more common when the system is filled with tap water instead of the recommended products. In regions

with crevices and corners, such as those found in the fitting of tubes, these incrustations can lead to the phenomenon of crevice corrosion, in which the adhered material has low cohesion and can be removed by the passing fluid, taking with it chunks of the passivating layers and exposing the bare metal. This type of corrosion, very common in stainless steels with low nickel contents (Sulzer Pumps, 2010), may have been the main corrosion mechanism contributing to the cracks observed.

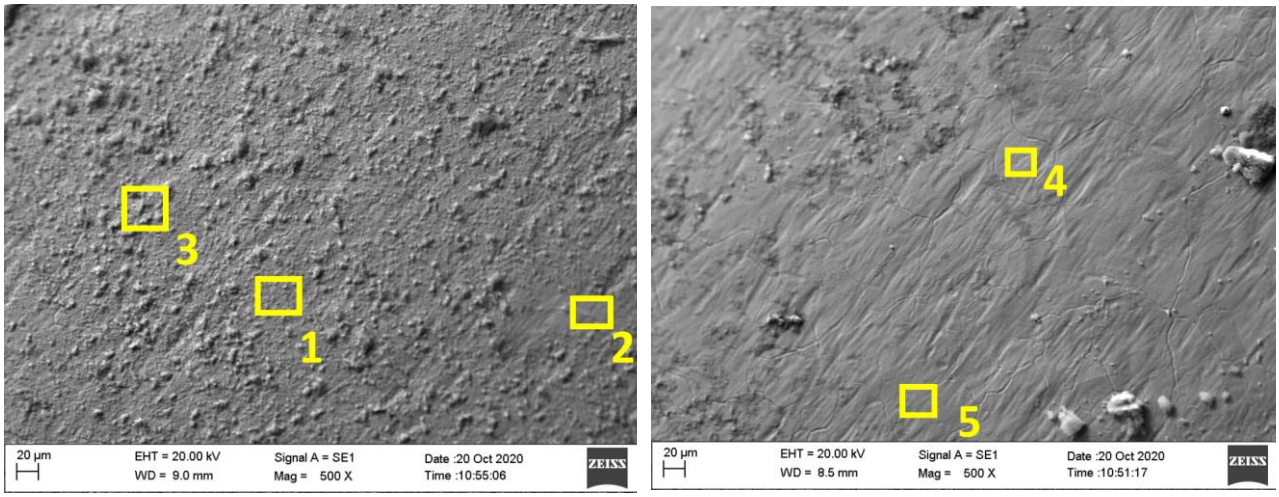


(a) (b)

Figure 7. (a) SEM image of the oxidized region of the tubes and (b) non-oxidized region.

The unoxidized region, in Fig. 7b, represents the base metal of the radiator tubes, which has a chromium content around 17%, nickel above 6% and manganese below 2%. According to ASTM A240 (2020), this composition is typical of AISI 300 series austenitic stainless steels, which indicates a greater chance that the tube material is AISI 301 steel, for example, due to the lower nickel content compared to the other steels in the series; or even AISI 304 steel, which is more common and cheaper, although in this case it would have nickel below the standard required. In any case, the material characteristics for this application would not be adequate. The ASTM A632 (2019) standard recommends that in applications where corrosion resistance is required, AISI 301 steel should not be used, and that 304 should strictly meet the nickel content between 8 and 11%. Since this element hinders the occurrence of the corrosion mechanisms mentioned by increasing the stability of the passivating layer (Azuma et. al., 2004), its presence below the recommended minimum contributed to equipment failure.

Table 1. Chemical composition of the EDS analysis of the regions indicated in Fig. 6.

| area | O | Al | Si | Cr | Mn | Ni |
|---|---|---|---|---|---|---|
| **1** | 25.8 | 9.9 | 0.3 | 11.2 | 1.0 | 3.9 |
| **2** | 13.1 | 4.6 | 0.5 | 15.1 | 1.3 | 5.4 |
| **3** | 32.7 | 13.0 | 0.4 | 8.7 | 0.9 | 2.9 |
| **4** | 5.1 | 0.8 | 0.6 | 16.3 | 1.7 | 6.3 |
| **5** | 4.0 | 0.6 | 0.5 | 17.4 | 1.7 | 6.5 |

The microstructure images of the tubes are shown in Fig. 8, whereas the first two were obtained for the samples etched with $FeCl_3$, which reacts only at the grain boundaries and twinning regions, as pointed by the red arrows. These images show the microstructure of the tubes in their original state after lamination, for which the high strain produces more irregular and finer grains near the surface, as can be seen in Figure 8(b) at the borders of the section. In Figure 8(c), another portion of the grinded and polished sample was attacked with a mix of HCl and $HNO_3$, showing some textured grains typical from martensite and pearlite structures. Also, although Figure 8(d) was obtained after etching the annealed sample for 3 minutes without prior grinding or polishing, which complicated the visualization of the grains, the austenite phase could be distinguished again, since it is more homogenously attacked by the acid and creates a more reflective surface. The twining barriers pointed are the characteristic trait of this phase, since it only occurs in Faced Centered Cubic system. On the other hand, the darker structure are a likely result of a heterogeneous attack that usually happens in lamellar structures such as pearlite and martensite.

The large size of the grains is also notable, which is a result of the annealing treatment. Although austenite is the predominant microstructure of the AISI 300 class of stainless steels, it is possible that the heat treatment also promoted diffusion of nickel and chromium to the grain boundaries, which would favor formation of the α phase in the form of pearlite. Other possibility is that the sawing and opening of the tubes promoted martensite transformation at some regions from the original austenitic grains, which is a common phenomenon when the grain undergoes high mechanical stress (Smallman and Ngan, 2014). In both cases, the slow cooling process at the oven favors the diffusion of carbon out of the austenitic grains, which tends to form carbides with the alloying atoms. This phenomenon is consistent with the distinctive grain boundaries pointed in Fig. 8(d).

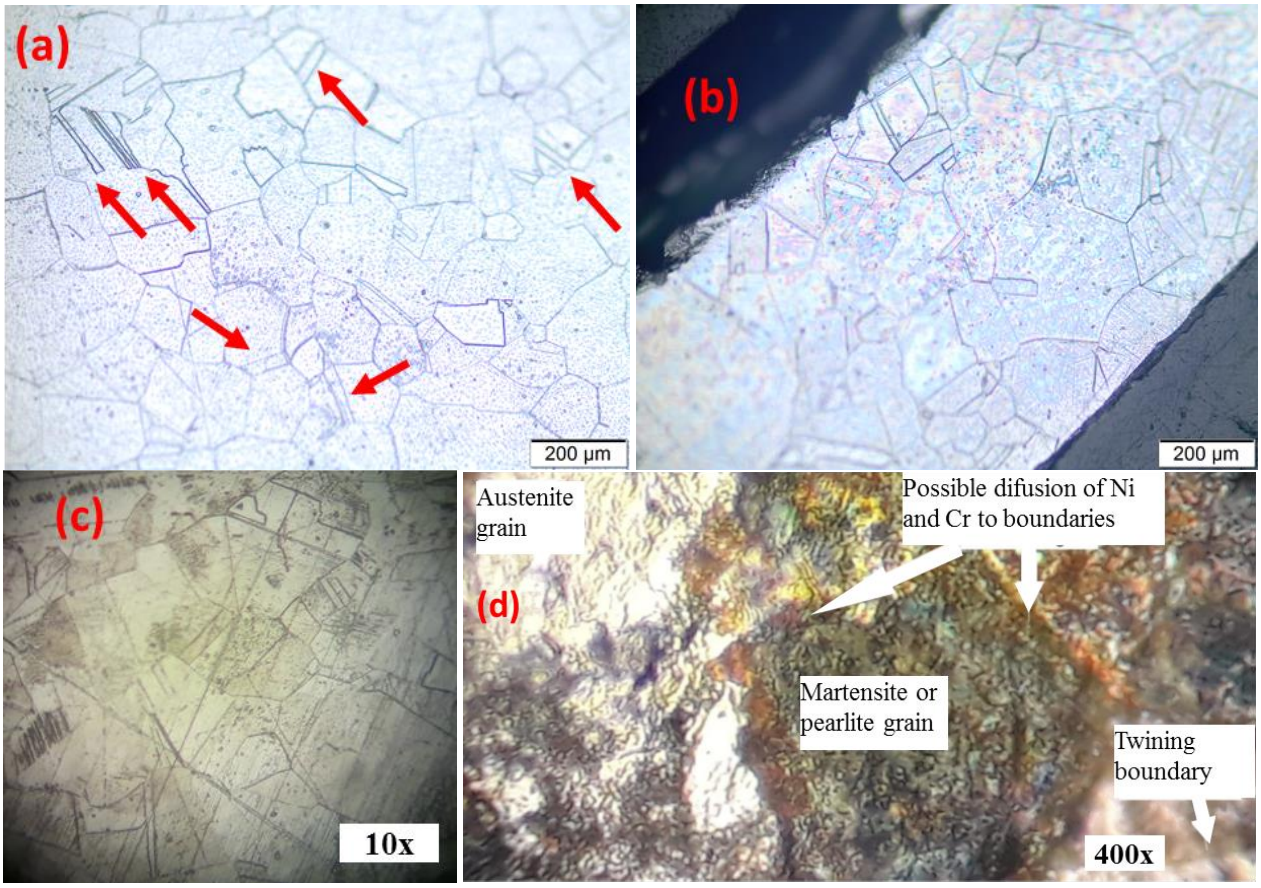


Figure 8. Microstructure of the internal stainless steel tubes of EGR radiator. (a) Twinning phenomenon and (b) refined grain at borders of section due to high strain in sample grinded, polished and etched with $FeCl_3$. (c) Textured darker grains possibly from martensite or pearlite phases in sample grinded, polished and etched with HCl and $HNO_3$. (d) Possible diffusion of Ni and Cr in annealed sample etched with 20 % HCl with no prior grinding nor polishing.

In the case of the radiator box plate, the SEM images are shown in Fig. 9, with much less oxides adhered to the surface. The chemical composition for different regions is shown in Tab. 2. It is observed that the nickel content between 9 and 10%, chromium on average 21.3% and the absence of molybdenum are close to steel AISI 304. Also, according to ASTM A666 (2015), it is recommended that this material in the annealed condition has a minimum hardness of 92 HRB, which is equivalent to 88.6 HR15T according to ASTM E140 (2019) in relation to austenitic stainless steels. This last scale was used in the tests due to equipment limitations, resulting in an average hardness of 98.6 HR15T of the EGR box material, which meets the standard specifications. In fact, it was observed that corrosion occurred mainly in the tubes and at their junction with the side plate of the box, with less intensity on the box structure itself. This behavior indicates that the higher nickel content of this part of the equipment was efficient in reducing crevice and pitting corrosion. Thus, one can also relate leak failures to the choice of pipe material during manufacturing planning.

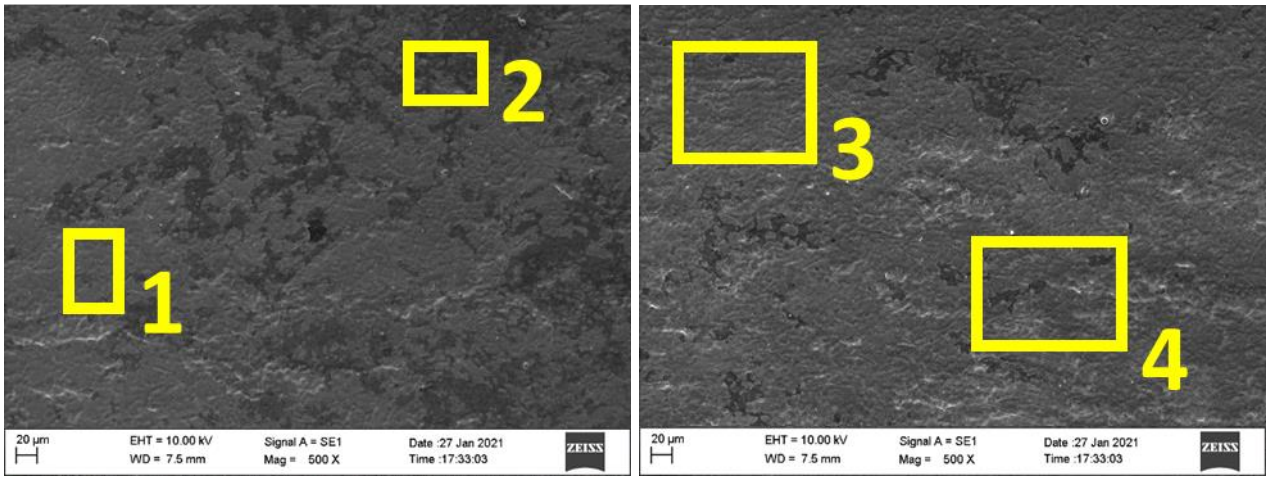


Figure 9. SEM image of different regions in the sheet of the radiator box, showing less oxidation.

Table 2. Chemical composition in regions on EGR radiator box plates. Empty cells indicate that the element was either absent or in little undetectable quantities.

| area | O | Al | Si | Cr | Mn | Ni |
|---|---|---|---|---|---|---|
| **1** | | 0.5 | | 22.6 | | 9.9 |
| **2** | 2.4 | | | 16.3 | | 10.9 |
| **3** | | | 0.5 | 25.2 | | 9.2 |
| **4** | | | | 21.0 | | 10.4 |

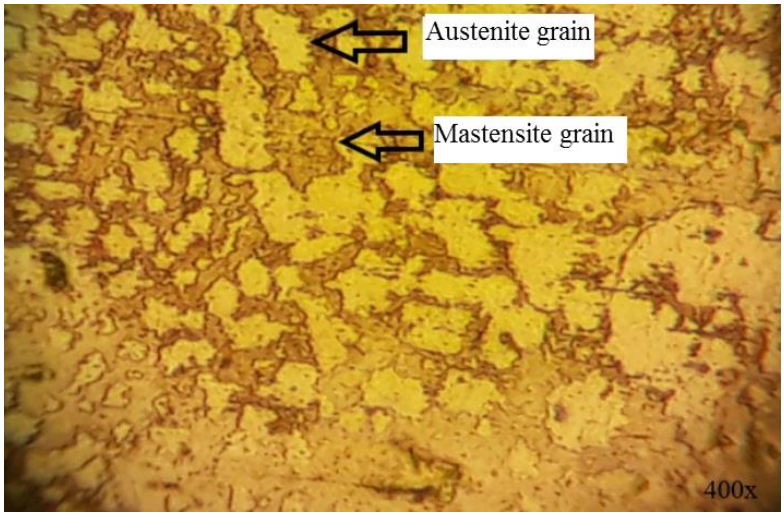


Figure 10. Microstructure of the stainless steel sheet of the outer box of the EGR radiator, showing distribution of austenite (clearer) and possible martensite (darker) grains.

Regarding the microstructure of the sheet that makes up the box of the radiator, the appropriate grinding and polishing together with reduced time for chemical attack significantly improved the visualization of the grains. Also, since the sheet samples were not annealed, the grains are conserved in their original smaller size, typically obtained in the rolling of steel sheets (Callister and Rethwisch, 2018). Again, the clearer grains show the predomination of the austenitic structure, with smaller darker areas where martensitic structure is possibly present.

## 4. CONCLUSIONS

The exhaust gas recirculation system (EGR), an important component for reducing NOx emissions in diesel vehicles, was investigated in this work regarding the occurrence of a critical leak failure in a national truck manufacturer. The root cause analysis and investigations regarding the type of material in the part allowed the following conclusions:

• Leaks in the EGR radiator occurred primarily in cracks present in the fittings of the inner tubes to the external plates of the radiator box and, to a lesser extent, in small holes along these tubes;

• The small holes originated in pits of corrosion resulting from the punctual removal of the passivating layer in the pipe material, possibly accelerated by the high temperatures and by the presence of chlorine ions resulting from the incorrect supply of the cooling system with tap water;

• Residual stresses resulting from the manufacturing process and high exhaust gas temperatures contributed to the appearance of cracks observed in the fitting of the tubes, which may have been accelerated by the presence of aluminum salts and chloride traces present in the water from the cooling system;

• Crevice corrosion was the predominant mechanism causing the leaks, with pit corrosion as a secondary mechanism;

• The nickel content in the tubes below that recommended by ASTM standards was an important factor in facilitating the mechanisms of crevice and pitting corrosion;

• It is recommended to change the material of the tubes to an austenitic steel with higher nickel content, such as AISI 316, in order to increase the corrosion resistance of the tubes at high temperatures in the possible presence of salts and chlorine ions, aluminum, among others.

## 5. ACKNOWLEDGEMENTS

The authors are thankful to the University Center UNA in Uberlândia and the Multiuser Microscopy Laboratory of the Faculty of Chemical Engineering in the Federal University of Uberlândia for the support in carrying out the tests.

## 6. REFERENCES

ASTM A240/A240M-20a, 2020. "Standard Specification for Chromium and Chromium-Nickel Stainless Steel Plate, Sheet, and Strip for Pressure Vessels and for General Applications". *American Society of Testing and Materials*.

ASTM A632-19, 2019. "Standard Specification for Seamless and Welded Austenitic Stainless Steel Tubing (Small-Diameter) for General Service". *American Society of Testing and Materials*.

ASTM A666, 2015. "Standard Specification for Annealed or Cold-Worked Austenitic Stainless Steel Sheet, Strip, Plate, and Flat Bar". *American Society of Testing and Materials.*

ASTM A1047/A1047M-05, 2019. "Standard Test Method for Pneumatic Leak Testing of Tubing". *American Society of Testing and Materials.*

ASTM E140-12b, 2019. "Standard Hardness Conversion Tables for Metals Relationship Among Brinell Hardness, Vickers Hardness, Rockwell Hardness, Superficial Hardness, Knoop Hardness, Scleroscope Hardness, and Leeb Hardness". *American Society of Testing and Materials.*

Azuma, S., Kudo, T., Miyuki, H., Yamashita, M., e Uchida, H., 2004. "Effect of nickel alloying on crevice corrosion resistance of stainless steels". *Corrosion Science*, Vol. 46, No. 9, p. 2265-2280.

Callister, W. D., & Rethwisch, D. G., 2018. *Materials science and engineering: an introduction*. John Wiley & Sons, New York, 9th ed.

Conselho Nacional do Meio Ambiente-CONAMA, 2018. "Resolução nº 490, de 16 de dezembro de 2018", *Diário Oficial da União*, Vol. 223, p. 153.

Conselho Nacional do Meio Ambiente-CONAMA, 2018. "Resolução nº 492, de 20 de dezembro de 2018", *Diário Oficial da União*, Vol. 246, p. 141.

DIN EN 1779, 1999. "Non-destructive testing - Leak testing - Criteria for method and technique selection". *European Standards*.

Janikowski, D. S., & Blessman, E. R., 2008. "Manufacturing and Testing of Welded Stainless Steel Tubing: You Have a Choice Part 2—Feedwater Heater Tubing". *In ASME Power Conference*, Vol. 48329, p. 381-393.

Janikowski, D. S., 2012. "Selecting Feedwater Heater Tube Materials for Greatest Efficiency and Reliability". *API Power Chem*, Terrigal, NSW.

Mukahiwa, K., Bertali, G., Burke, M. G., Duff, J. e Scenini, F., 2019. "The beneficial effect of surface carbon coating on stress corrosion cracking of Type 304 austenitic stainless steels in high temperature water". *Scripta Materialia*, Vol. 158, p. 77-82.

Papavinasam, S., 2014. *Corrosion Control in the Oil and Gas Industry*, Elsevier, London, UK, 1st ed.

Pradhan, S. K., Bhuyan, P. e Mandal, S., 2019. "Influence of the individual microstructural features on pitting corrosion in type 304 austenitic stainless steel". *Corrosion Science*, Vol. 158, p. 091-108.

Pumps, S., 2010. *Centrifugal pump handbook*. Butterworth-Heinemann, Winterthur, 3ª ed.

Smallman, R. E. & Ngan, A. H. W., 2016. *Modern physical metallurgy*. Butterworth-Heinemann, Oxford, 8th ed.

Yuan, X., Liu, H., e Gao, Y., 2015. "Diesel engine SCR control: current development and future challenges". *Emission Control Science and Technology*, Vol. 1, no. 2, p. 121-133.

Zamboni, G. e Capobianco, M., 2012. "Experimental study on the effects of HP and LP EGR in an automotive turbocharged diesel engine". *Applied Energy*, Vol. 94, p. 117-128.

Zhu, L. K., Yan, Y., Qiao, L. J. e Volinsky, A. A., 2013. “Stainless steel pitting and early-stage stress corrosion cracking under ultra-low elastic load”. *Corrosion science*, Vol. 77, p. 360-368.

## 7. RESPONSIBILITY NOTICE

The authors are the only responsible for the printed material included in this paper.